# Dynamic modeling and state estimation of cable-conduit actuation during interaction with non-passive environments

Stephen Buchanan, Fabrizio Sergi, Member, IEEE

Abstract—Remote actuation solutions such as cable-conduit transmissions are beneficial in wearable robotics to reduce dynamic loading on distal joints. However, these systems often introduce high reflected impedance or require rigid sensors for force control that hinder their integration in wearables. Low impedance and ease of integration could be both obtained by combining distributed cable strain sensing with dynamic modeling to estimate output force and position.

In this paper, we present a new computational model to analyze the dynamics of cable-conduit systems. The model features bi-directional propagation of motion within the transmission, which allows for simulation of human-interacting systems where either or both the human and the robot can be force or position sources. Moreover, we present a new method for rapidly solving for the system of equations based on iterative linearization of the system of nonlinear equations. The model and solution method are validated in a physical prototype through experiments involving physical interaction with a human subject. Finally, we develop methods for model-based estimation of cable tension given measurements from multiple noisy strain sensors embedded in the transmission, and quantify the accuracy achievable via different methods as a function of the number and location of sensors.

Results demonstrate that the model accurately predicts behavior observed in the prototype. Moreover, the newly developed iterative linearization solution method allows a 100-fold increase of computation speed compared to a standard solver. Finally, we demonstrate that cable tension can be estimated with increasing accuracy when increasing the number of sensors, but accuracy decreases if the output portion of the transmission is not instrumented.

# I. INTRODUCTION

Wearable human-interacting robots frequently employ remote actuation, as remote actuation allows for the optimization of actuator placement to minimally affect the dynamics of the limb being manipulated [1].

Cable-conduit transmissions, which employ a fixed outer sheath and mobile inner cable, are a common choice for remote actuation due to their flexibility, low mass, and ability to withstand large forces. However, the nested cable design introduces non-negligible frictional losses and mechanical compliance. Consequently, the transmission suffers from diminished mechanical efficiency and backlash, leading to input-dependent stability properties [2]. Moreover, friction increases the reflected impedance of the system. While friction can be reduced by proper design, these effects remain

We gratefully acknowledge the support of the National Science Foundation via grant no. 1638007, and of the UNIDEL foundation through the Henswear initiative.

S.B. and F.S. are with the Human Robotics Laboratory, Department of Biomedical Engineering, and with the Department of Mechanical Engineering. University of Delaware, Newark, DE 19713.

Corresponding author (F. S.): (fabs@udel.edu)

significant enough that the system exhibits poor tracking performance without proper compensation.

Many existing human-interacting robots utilizing cable-conduit transmissions employ only a single cable, allowing the cable to be slackened when the desired torque is zero [3], [4], [5]. However, single-cable systems can only apply torque in one direction. While systems that use two cables have bidirectional torque transfer capabilities, these systems also require more careful control since slackening both cables to achieve zero torque is not possible without complicated and dedicated hardware solutions [6]. As such, usually distal cable tension [7] or single-axis torque [8], [9] sensors are used for feedback control.

Numerous specialized feedback laws for frictional effects present in cable conduit systems have been proposed over the years, including linear and non-linear formulations, such as force control with integral feedback [10], position control with approximation of backlash-like hysteresis [11], and torque controllers [12], with double sheath configurations [13]. However, all these controllers are based on simplified models using Coulomb friction, which assume a constant cable configuration or interaction with a passive environment. Using a more accurate model in a feedback controller could allow for improved system performance in applications involving human-robot interaction.

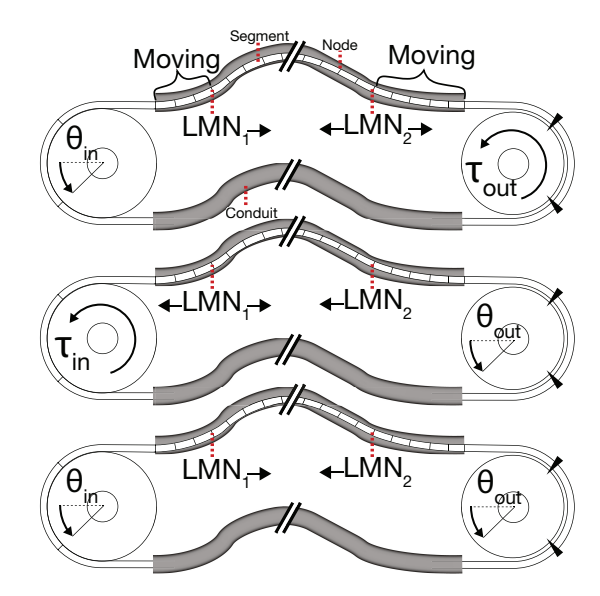


Fig. 1. Schematic of the cable-conduit dynamic model presented in this paper, featuring all 3 operating modes (Position-Torque, Torque-Position, Position-Position). Note the model's ability to change the number of mobile cable segments at both ends of the conduit, as appropriate.

Early dynamic models of the cable-conduit transmission pursued a lumped-mass approach, approximating the inner cable as a series of interconnected mass-spring-damper systems [2], [14]. These models provided reasonably accurate estimations, but were constrained to constant curvature, pretension and environment stiffness. These lumped-parameter models were later improved upon by Palli & Melchiorri [15] who used the dynamic Dahl friction model. Do et al. [11], [16], [17] further improved the accuracy of friction estimation by studying a wide array of models and selecting a modified Bouc-Wen model.

Agrawal et al. [18], [19] proposed a distributed model based on a set of partial differential equations for a cable subject to arbitrary curvature. Their new formulation allowed for the study of pull-pull cable systems, and reproduces the phenomenon of partial movement within the cable, where only one region of the cable is under motion. Their derivation, however, constrained the model to the study of systems that interact with passive environments and are position-controlled at their input. These limitations are highly restrictive for the study of practical systems. Typical input actuators, such as DC motors, are torque regulated, not position regulated which leads easier implementation of force-control over position-control. Additionally, assuming interaction with a passive environment imposes that motion can only propagate in a single direction in the cable. Fig. 1 shows that when considering active environments motion will need to propagate in both directions. Since human-robot interaction focuses on the interaction with active environments, models of cable-conduit transmissions for humanrobot interaction must not assume monodirectional motion propagation.

A beneficial use of a dynamic cable transmission model is for the implementation of model-based control. In this scenario, given measurements of some of the system states, the controller can determine the exact amount of the inputs required to satisfy a certain control objective (i.e. desired force or position). Problems associated with model-based control for cable transmissions are the limited capability to measure the progression of states distributed through the cable in real-time. There have been many recent developments on the measurement of cable tension and displacement along the cable in real time, such as the measurement of curvature through optics [20], to measure bend radius, or custom Halleffect sensors [21] to measuring displacement, or the use of piezoresistive sensors to measure cable strain [22], and even on combing force and Hall-effect sensors to measure both tension and curvature [23]. These studies incorporated state measurements into standard feedback controllers, ranging from basic closed loop PI controllers to Impedance control or Force feedback controllers. However, it is unclear how measurements from a redundant set of sensors located in some nodes along the cable can be used to derive an estimate of the entire set of system states, which would enable modelbased dynamic compensation.

Previous work [24] extended the model of Agrawal et al. [18], [19] by developing a new formulation to solve for the

complete state of the cable-conduit system in the presence of any two applied tensions or displacements. As such, the model is capable of propagating motion from either side of the cable, in both directions, concurrently, to describe the interaction with non-passive environments. Moreover, we previous present a new method for rapidly solving the system of equations of cable-conduit systems based on iterative linearization of the non-linear system of equations produced by the model, which enables real-time simulation.

In this manuscript, we first cover a brief overview of the model and linearization solver, then present new methods developed for model-based estimation of cable tension, given measurement from multiple noisy strain sensors distributed within the transmission, and quantify the accuracy achievable via different methods as a function of the number and location of the sensors.

#### II. METHODS

### A. Model formulation

We developed a dynamic model of the transmission based on the assumption of an axially linear elastic cable. The model formulation was fully presented in our previous work [24]; here we briefly recall the main aspects to allow presenting the novelty aspects included in this contribution.

The dynamic model is based on a finite element approach. The cable is divided into N discrete segments, where system parameters such as radius of curvature are approximated as constant. When in tension, a given segment of cable experiences frictional losses in tension due to contact between cable and sheath. For an infinitesimal element of length dx, tension at each node  $T_i$  creates a normal force  $F_n$  between cable and conduit at a given point as a function of the radius of curvature R(i), given by  $F_n \approx T_i R(i)^{-1} dx$ . Normal force  $F_n$  is assumed to be constant over the given segment's length  $\Delta x$ . Normal force can be multiplied by coefficient of friction  $\mu(v_i)$ , a function of segment velocity  $v_i$  and direction of motion  $S_i = \text{sign}(v_i)$  respectively, then integrated along the cable. The result is that the ratio between the tension at the two nodes of the cable segment  $T_{i+1}/T_i$  is given by:

$$\frac{T_{i+1}}{T_i} = \exp\left(\frac{\mu(v_i)S_i\Delta x}{R(i)}\right),\tag{1}$$

as demonstrated by [19].

Additionally, since the cable is modeled as an elastic element with spring constant  $K_c$ , Hooke's Law provides a relationship between the change in tension across a segment due to friction and the change in length of the segment,

$$u_{i+1} - u_i - \frac{R(i)S_iT_i}{K_c\mu(v_i)} \left[ \exp\left(\frac{\mu(v_i)\Delta x S_i}{R(i)}\right) - 1 \right] = 0$$
 (2)

where  $u_i$  and  $T_i$  represent the displacement of and tension at node i. These two equations fully define the state of all moving segments in the cable, and are evaluated at each timestep during simulation for segments i = 1 to k - 1.

During operation, before the cable is in tension, the tension has to propagate along the cable form the motion source, leaving some nodes stationary. If a node is stationary, its tension and position cannot change from one iteration to the next. When a stationary node  $k \pm 1$  is adjacent to the "last moving node" (LMN) k, a boundary condition for the motion of the mobile segment(s) of cable is given by

$$u_k + \frac{T_k \Delta x}{2K_c} = u_{k\pm 1} - \frac{T_{k\pm 1} \Delta x}{2K_c} \tag{3}$$

The equations above yield 2k-1 equations while in partial motion, or 2k-2 equations during mass motion (i.e., all segments are moving), but there are 2k free variables (k each of position, tension) defining the cable state. To solve the system, at least two additional constraint equations are required. These equations specify either the exact value of a variable (e.g. a known position, or tension), or relate two variables in a way not linearly dependent with existing equations (e.g. an equation representing a position-tension relationship of a spring connected to the output of the system). Furthermore, two modeled cables can be connected to a load pulley in a pull-pull configuration by including appropriate constraints on their end positions, allowing the modeling of bidirectional motion as a single cable can only provide monodiriectional motion by pulling force.

The equations above pertain to the static or dynamic conditions within the cable. However, a key element of cable-conduit system is the transition between these conditions i.e. motion propagation. Motion propagates through the cable when a stationary node  $k\pm 1$  on the cable becomes the new LMN, k. This condition is verified when the difference in cable tension at that node can overcome friction,

$$T_{k\pm 1}S_k \ge T_k S_k \exp\left(\frac{\mu(v_i)\Delta x S_k}{R(n)}\right)$$
 (4)

A change in LMN means that an additional segment would have moved during the previous time instant, and requires re-evaluation of the dynamic equations, iteratively, until the assumed value of k coincides with the one derived based on the dynamic equations. The LMNs reset to the first and last node when motion stops or changes direction, since every segment will be required to change direction at these instants.

Lastly, in the event that a segment becomes slack, (i.e. it has non-positive tension), our model neglects any contributions from this segment until it is no longer slack, which happens when its calculated tension is greater than zero.

1) Definition of inputs and outputs: To solve the system of equations, we specify at least one position or force at the input side, and one position or force at the output. In theory, this could be done using any pair from the set  $\{u_1, u_{N+1}, T_1, T_{N+1}\}$ . However, the system is fully defined only if the input pair specifies at least one position variable. Otherwise, the system of (1,2) requires an additional equation that maps the total applied force to the cable to its acceleration, a phenomenon that is not captured in our quasi-static model, to calculate absolute positions instead of relative ones. As such, we do not consider the couple  $\{T_1, T_{N+1}\}$  for the purposes of this paper.

The possibility of imposing variables at both the input and output side of the cable allows us to study interaction with non-passive environment. As a result, the model cannot assume motion will always propagate from the proximal end of the cable to the distal end. To accommodate this, the model introduces a second last moving node, k', which can propagate from the distal side of the cable back toward the proximal end. When k and k' do not coincide, each end of the cable is treated as a separate system and solved independently, since no motion or tension can be transmitted through non-moving nodes. When the two moving nodes k and k' coincide, the cable begins to undergo mass motion and is solved as a single system.

2) Friction modeling: Our model specifies the friction coefficient  $\mu$  for a given segment i as a function of that segment's velocity,  $v_i$ , calculated at the previous timestep as

$$v_i = (\dot{u}_i + \dot{u}_{i+1})/2 \tag{5}$$

Our friction model is based on a simple stiction model

$$\mu(v_i) := \begin{cases} \mu_s & \dot{v}_i = 0\\ \mu_d & \dot{v}_i \neq 0 \end{cases} \tag{6}$$

for all presented analyses, except where otherwise specified.

#### B. Linear solver formulation

The model exists as a set of nonlinear equations with a unique numerical solution; however it is likely that a closed-form solution for the system state variables will not be found. In general, numerical solutions for nonlinear equations can be found via iterative optimization. Two important properties of this class of solvers are: *i*) no assurance that it will provide a solution within desired tolerance bounds; *ii*) no guarantee of convergence within a given number of iterations or within a given computation time.

These properties are not desirable for any simulation, and especially so for real-time applications. The possibility of finding no solution, or worse, an incorrect solution, is problematic for the robustness of any controller utilizing that solver. Additionally, the time costs of such an algorithm are unacceptable. In preliminary testing, the rate of solution did not approach speeds needed for real-time control using standard hardware.

To formulate a faster solver for this dynamic model, we take note of the form of equations described in Sec. IIA. Those equations are nonlinear as a function of the unknown states  $T_i$ ,  $u_i$  and their derivatives, solely because of the presence of the sign function, which has node velocity as an input. As such, we can introduce a simplification to bypass the non-linearity introduced by the sign $(v_i)$  function. Despite a continuous range of inputs, the sign function assumes only three distinct values: 0 (for  $v_i = 0$ ), 1 (for  $v_i > 0$ ), and -1 one (for  $v_i < 0$ ). Also, while there are 2N equations, there are only N distinct arguments to the sign function, i.e. one per each segment. The set of possible systems with the equations of motion amounts to  $3^N$ , i.e. equals the number of possible permutations of the values of the N sign functions included in the equations. Such an exponential scaling with the number of parameters, however, undesirable, as in the case of a cable with only 5 segments, there would be as many as 243 possible different systems of equations. However, there are useful properties to exploit.

First, many of these permutations are physically impossible for this model. Consider a 5-segment cable whose sign functions output the set [-1,1,1,1,-1]. This configuration cannot, in fact, exist - the lack of inertia in the model means that wave propagation is impossible. As such, motion in the cable must be described completely by 3 regions: i), one moving in the same direction as node 1 and extending from node 1 to the unknown node k, ii), one moving in the same direction as the node N+1 and extending from node N+1 to the unknown node k', iii) one stationary region in the center of the cable. This observation rules out several permutations defined in terms of segment motion, reducing the number of admissible permutations to a value  $n_p^* = 2N+1+\sum_{j=1}^{N-1} 4j$  which scales polynomially with N. A derivation of this result can be found in Appendix I.

Second, another simplification arises from the fact that tension and displacement are unaltered within a stationary section of the cable. As such, a configuration with two distinct moving cable sections can be solved in a simplified form by splitting the cable in two sections under mass motion, which generates a linear system with less than 2N equations.

As such, recalling that the *only* nonlinearity present was the sign function, we start by assuming arbitrary initial conditions for  $\operatorname{sign}(v_i)$ , and proceed with solution of the now linear, algebraic set of equations. We test the solution (if one exists) for validity of the assumptions made, and repeat (up to  $n_p^*$  times) until all the assumptions are verified, and thus the solution is considered to be the correct one. While it doesn't follow trivially that this solution method is guaranteed to provide the unique solution of the system of nonlinear equations, a proof is provided in Appendix II.

#### C. State estimation

While all states of the system can be estimated provided a measurement of force or position at the input and output, the sensing condition referenced above is not always possible or desirable. In some applications, such as those involving wearable robots, the use of a F/T sensor at the distal end can be inconvenient as it would increase the weight of the device and require rigid materials. However, if distal measurements are completely missing, the system is under-defined under mass motion, making solving for the system states impossible. A solution to this problem could be to include strain sensors along the cable, such as carbon nanotubes [22], to measure local cable deformation or curvature. This solution requires state estimation, where the model is simulated by combining multiple redundant sensor measurements to estimate the entire states of the system.

We developed a model-based state estimator by adapting the linear solver referenced in Sec. IIB to allow for data to be entered at any node along the cable, rather than only input and output tension or displacement as discussed above. In theory, any pair of inputs representing position and/or tension measured at non-stationary nodes, when used as input to the solver, is guaranteed to provide the correct estimate if the direction of motion is known for the entire cable. However, if measurements are available with uncertainty, and/or if the direction of motion is not known a-priori, it is likely that the states of the system will be estimated with error. To reduce the effects of uncertainty, it may be convenient to use a redundant set of sensors, and to combine repeated model-based state estimations. Because fusion of the results of multiple model-based state estimation methods will differ based on whether the direction of motion is known or not, we developed two different approaches. As it is often practical in real world applications, in all our estimators we also always assume to have perfect knowledge of the displacement of the motor-side of the cable (i.e.  $u_1$ ). As such, each modelbased state estimation will be obtained by pairing a noisy tension measurement available at a given cable node with the measurement of  $u_1$ .

1) Direction of motion known: In this case, we assume that the direction of motion in all segments in the cable is known with infinite accuracy. Assuming availability of m tension measurements at nodes  $M = \{i_1, i_2, ..., i_m\}$ , at each iteration, each measurement j = 1, 2, ..., m is paired with  $u_1$  to yield an estimate of the system states  $T^{(j)}$  and  $u^{(j)}$ . For each model-based estimation, the linear solver is confined to solutions under the true direction of motion. The resulting estimate of the system states is obtained by averaging the independently estimated profiles  $T^{(j)}$  and  $u^{(j)}$ .

2) Direction of motion unknown: In practice, we cannot assume that we have knowledge of the direction of motion of each cable segment. Estimation performed without knowledge of direction of motion is more likely to incur in estimation errors, as use of incorrect values for parameters  $S_i$  in (1) and (2) leads to conducting state estimation using an inaccurate system of equations of motion.

To estimate the system's states when the direction of motion is not known, we obtain a first guess of the m estimates  $T^{(j)}$  and  $u^{(j)}$  by running the model-based solver with the available measurements, using as initial guess the direction of motion estimated at the previous iteration. However, in this case, the estimates are not forced to comply with the assumed direction of motion, and the linear solver is repeated until the assumed and calculated directions of motion match. The output of this process is a set of estimated states  $T^{(j)}$ and  $u^{(j)}$ , and direction of motion vectors  $v^{(j)}$ , where each element in v equals 0, -1 or 1. The coordinates of the last moving node LMN $^{(j)}$  on either side of the cable are uniquely associated to the direction of motion vectors  $v^{(j)}$  as the first and last node with estimated  $v^{(j)} = 0$ . Given  $v^{(j)}$ , the consensus on the direction of motion is established as the *median* of all  $v^{(j)}$  values, with an associated consensus for the two LMN. When sensors are located in nodes corresponding to a stationary region (comprised between two last moving nodes), their readings are removed and not used for sensor fusion. We developed four methods to combine the estimates  $T^{(j)}$  and  $u^{(j)}$  with the direction of motion consensus to estimate the system states, as described below. The weight used is an average of individual sensor profiles over multiple iterations further discussed in Sec. IIIC

Mean Average the profiles  $T^{(j)}$  and  $u^{(j)}$  as done for the known direction of motion case.

Mean-R Average the profiles  $T^{(j)}$  and  $u^{(j)}$  only considering nodes where  $v^{(j)}$  agrees with the consensus.

W Mean Apply a weighted average of the profiles  $T^{(j)}$  and  $u^{(j)}$ , using as weights measurements of sensor-specific estimation accuracy (see Sec. IIIC).

W Mean-R Apply a weighted average to profiles  $T^{(j)}$  and  $u^{(j)}$  only considering nodes where the estimated  $v^{(j)}$  agrees with the consensus.

# III. METHODS VALIDATION

#### A. Model validation

Previous work [24] developed a test platform to include a cable-conduit transmission between a DC motor and a handle constrained to apply torques along the flexion/extension axis of a human wrist (Fig. 2). In this scenario, the human would apply effort to accomplish motion and the remote actuator would be controlled so as to display desired force/torque at the point of interaction to display virtual dynamic environments.

In the platform, the cable mounting plates can slide to regulate pretensioning of the system. The system has a fixed transmission ratio R of approximately 5, specified by the ratio of radii between the load and motor pulleys. Torque is supplied by a DC motor (Maxon motors RE35, 90 W, p/n: 273756). Torque from the motor is measured via current sensing. For static tests, the load pulley can be locked to its support structure by a bolt such that the applied torque can be measured by the 6 channel force/torque sensor (ATI mini40, resolution 0.5 mNm, 4 Nm at full-scale output). Position can

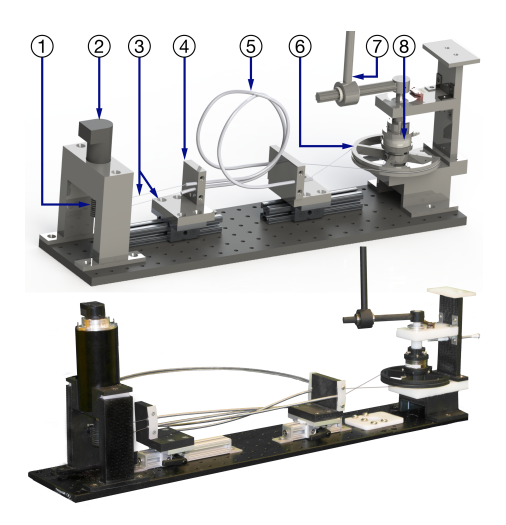


Fig. 2. Top: Rendering of test apparatus. The system is comprised of a motor (2) and its pulley (1), which drives two steel inner cables (3) through their conduits (5), causing motion of the load pulley (6) and of the handle (7). Mobile conduit supports (4) pretension the cable, and load torque is measured by a load cell (8). Bottom: Photograph of the physical prototype.

be measured at both ends via encoders present at both the actuator (2000 cpt) and load shaft (10000 cpt).

Each cable consists of a 2 m wound steel wire sheath with HDPE liner with an approximate inner diameter of 1.75 mm (Lexco Cable 408187), and an inner cable with a 7x19 stranded stainless steel core coated in nylon to a final outer diameter of 0.75 mm (Sava Cable 210149). The cables are arranged in a pull-pull configuration used to allow for bidirectional transmission of motion and force.

1) Parameter estimation: The model has eight parameters describing the mechanical properties of the system. Cable length, curvature radius, and both pulley radii were measured directly. The elastic coefficient of the inner cable was estimated by a measurement of the stretch-vs-force relationship for both cables in parallel with output pulley blocked. Pretension is calibrated using a spring stretched to prescribed lengths to move the cable mounts. The friction coefficients were estimated by minimizing the difference between model and physical results during a separate experiment. Table I lists the values provided to the model for each experiment, unless otherwise specified, where L represents cable length and K represents cable stiffness.

TABLE I
SYSTEM PARAMETERS USED FOR MODEL SIMULATION

L	R(x)	$r_{input}$	$r_{load}$	K	$T_0$	$\mu_d$	$\mu_s$
2 m	0.28 m	20 mm	104 mm	$2 \frac{kN}{m}$	10 N	0.21	0.63

2) Experiment 1: Sensitivity to parameter changes: In Experiment 1, we aimed to check that the model reacts correctly to changes in relevant physical parameters such as cable pre-tension and radius of curvature. To do so, the load pulley was locked, and the motor applied a torque alternatively ramping up and down with a slope of  $\pm 0.1$  Nm/s to a maximum of  $\pm 0.125$  Nm then dwelling for 0.5 s before reversing direction.

Under this paradigm, we studied variations in pretension. Pretension in the cables was set to 4 levels by using a spring stretched to different lengths to adjust the position of one cable mounting plate. The motor then applied its prescribed torque profile for 30s. The model was given the prescribed motor torque profile and fixed load angle as inputs. Only the pretension variable was changed in the model between trials. The results of this experiment are visible in Fig. 3. In agreement with (1), increased pretension is associated with increased friction, dead-width, and loss in torque transfer. This effect is visible both in the experiment and the model. From a quantitative standpoint, the output torque root-meansquare (rms) error obtained between model estimate and measurements is equal to 50 mNm, 10 mNm, 12 mNm, and 17 mNm for low, med-low, med-high, and high pretension parameters, respectively, with values equal to 20%, 5%, 8%, and 37% of the peak value. For comparison, a model neglecting distributed friction effects (i.e. output torque  $T_o =$  $r_{load}/r_{in}T_i$ ) would yield rms error values of 197 mNm, 244 mNm, 271 mNm, and 322 mNm, respectively. Overall, this

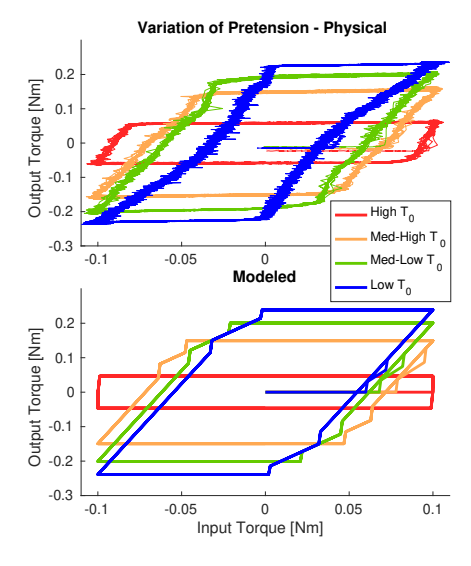


Fig. 3. Exp. 1: physical system and modeled behavior when pretension in the cables is varied. The model reproduces the trends in behavior introduced by variations in pretension correctly.

highlights the importance of modeling friction within the cable-conduit system

3) Experiment 2: Position-force mode: In Experiment 2, we validated our model's capability of capturing interaction with an active environment. Here, the motor is controlled to apply a torque  $\tau_m$  (newton-meters) in response to the angular displacement of the output  $\theta_o$  (in radians), given by

$$\tau_m(\theta) := \begin{cases} min(-\frac{1}{2}(\theta + 0.05), 0.2) & \theta < -0.05 \\ 0 & |\theta| \le 0.05 \\ max(-\frac{1}{2}(\theta - 0.05), -0.2) & \theta > 0.05 \end{cases}$$
(7)

During the experiment, the participant moved the handle periodically, imposing an amplitude of roughly 40 deg peak-to-peak. The trajectory imposed by the human and the corresponding requested motor torque were then input to the model which repeated the experiment in simulation in force-position mode, allowing to compare model estimates and experimental measurements of torque and position at the output and input pulley, respectively. Model parameters were left unchanged from Experiment 1. Fig. 4 shows the

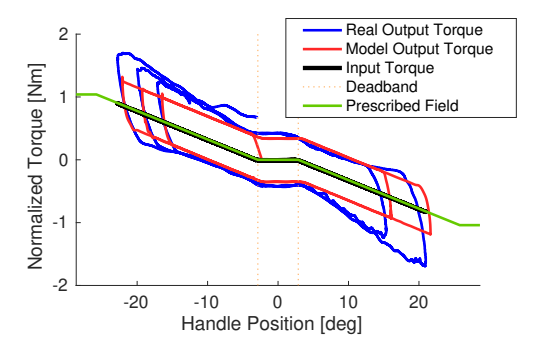


Fig. 4. Exp. 2: A comparison of the prescribed error-reduction tunnel and the measured torque when implemented naively with remote actuation. Accurate prediction of this behavior will allow for compensation of the effect.

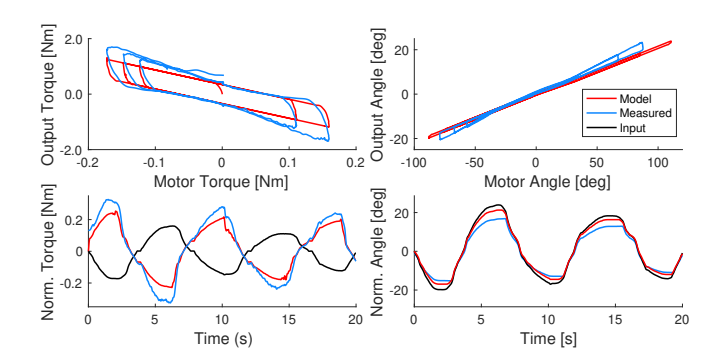


Fig. 5. Exp. 2: Simulated and measured error-reduction tunnel behavior. Torques and pulley angles have been scaled by the transmission ratio R in the lower plots.

hysteresis present in rendering of this virtual dynamic environment imposed by the transmission, both as captured by the experiment and simulation. Fig. 5 presents position and torque relationships both in the experiment and simulation. Overall, the figures suggest a qualitative match between experiments and simulations. For this experiment, the rms error in estimating the output torque was equal to 264 mNm, or 15.5% of the peak measured output torque. For comparison, a model neglecting distributed friction effects would yield an rms value of 539 mNm, or 31.7% of the peak measured torque.

While the model improves the estimate of output torque compared to ideal transmission models, there is a numerical discrepancy between the model and physical results. Some of this error can be attributed to shortcomings of the oversimplified stiction model used. We analyzed the behavior of the model in presence of a viscous friction term, and verified that the residuals (sum of squares of difference in torque values between simulated and experimental data) are reduced by about 50% (Fig. 6). It is expected that the use of a more advanced model will further reduce the residuals.

#### B. Linear solver validation

To test the relationship between the solution obtained using our simplified solver and iterative optimization based numerical packages, we compared the output of the solver described in Section IIB with the one obtained from the same model using MatLab's *fsolve* function. Both models implemented one cable with locked output connected via a spring (stiffness of 40 N/m) to a wall at i = N + 1 and were

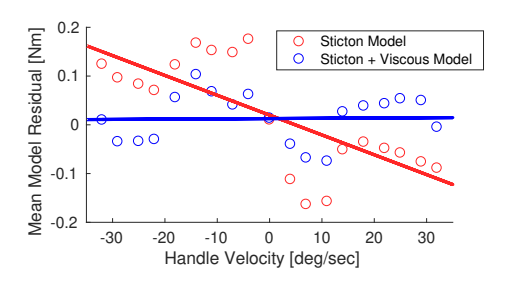


Fig. 6. Exp. 2: Comparison between model residuals, and their linear fits to velocity, with and without inclusion of a viscous friction term.

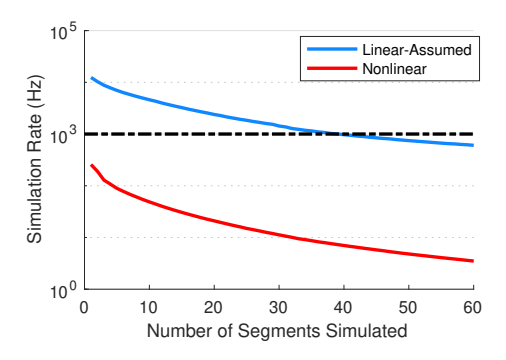


Fig. 7. Rate of model simulations (expressed as iterations per second) obtainable on the same computer, using either the presented solution method (linear-assumed) or using MATLAB's *fsolve* function (nonlinear).

simulated with a sinusoidal input position (amplitude of 0.15 cm) from the motor at i=1. The simulation used parameters from Table I, but with an increased preload of 40 N to offset slacking in the passive models. Both models were simulated over a range of parameter N (number of segments), up to 60, to observe their simulation rate at different number of segments.

The outputs of the implemented linear solver were identical to those of the non-linear solver within machine precision in all conditions, including mass motion, partial motion, mono- and bi-directional motion propagation (maximum error  $< 10^{-9}$  N), confirming the accuracy of the implemented solver. The results in Fig. 7 show that our linear solver outperforms the nonlinear solver by over two orders of magnitude in terms of computation speed on a desktop PC<sup>1</sup>, even when MATLAB's solver is programmed to use the previous solution as initial conditions for the next iteration. Since most control loops run at 1 kHz, the standard solver is not fast enough to run even a single segment simulation quickly enough, however our novel solver can simulate in real time up to a 40 segment cable within the window provided by a controller cycle. This analysis demonstrates that the linear solver is amenable for real-time simulation and control.

#### C. State estimation under measurement noise

We conducted a set of virtual validation experiments to validate the possibility of estimating cable tension based on measurements distributed along the cable. In these virtual experiments, we used the model to simulate the evolution of the system (considered as the "true value" of the system states), and compared the "true value" of the states to those estimated based on available sensor measurements. The model was simulated featuring a ten-segment cable, subject to sinusoidal input position (amplitude: 1 cm, frequency: 1 Hz, simulated at 100 samples per cycle), with a 10 N preload, in blocked output conditions with the same physical parameters as in Table I.

<sup>1</sup>Dell Precision T1700 Workstation, containing an Intel Xeon E3-1226v3 clocked to 3.30 GHz. MATLAB *bench* command reports the following reference times: LU: 0.1821s, FFT: 0.1256s, ODE: 0.0518s, Sparse: 0.1037s, 2-D: 0.2465s, 3-D: 0.2947s.

Sensor measurements were simulated for each node, assumed to arise from zero-mean guassian noise, with standard deviation comprised equal to 10% of the true value of the measurement. Simulated measurements were repeated 2000 times. For all repetitions, we ran the model-based estimators described in Sec. II were implemented, and quantified the absolute error between the model-generated true value of cable tension and values estimated based on measurements from noisy sensors.

To determine the effect of sensor noise and location on state estimation accuracy, we considered first the possibility of obtaining measurements from each sensor, one at a time. The results obtained from this analysis are primarily used to establish the appropriate weighting to use to each sensor estimate for sensor fusion. In addition, to evaluate state estimation in realistic sensing conditions and the possibility of sensor fusion, we also considered the following configurations, for every admissible value of the total number of sensors  $m \in (1,11)$ :

- 1) Even with m sensors evenly spaced throughout the cable (i.e. one each p nodes), starting from the proximal or distal node.
- 2) Distal m sensors only included at each node at the distal end of the cable.
- 3) Both m sensors present at each node at both the proximal and distal ends of the cable (m/2) at the proximal end, m/2 at the distal end).

We present the results of the analysis separately in the two following sections.

1) Single-sensor estimation: We conducted single-sensor estimation, estimated cable profiles  $T_i$  and  $u_i$  from individual sensor j, at two iterations corresponding to mass motion, one for positive and one for negative cable displacement. A representation of sensor-based estimate averaged over the 2000 estimations and showing the different in error between the positive and negative cable displacement iterations can be seen in Fig. 8.

We quantified the error function  $e_{ij}$  computed as the absolute estimation error of tension at node j when sensor

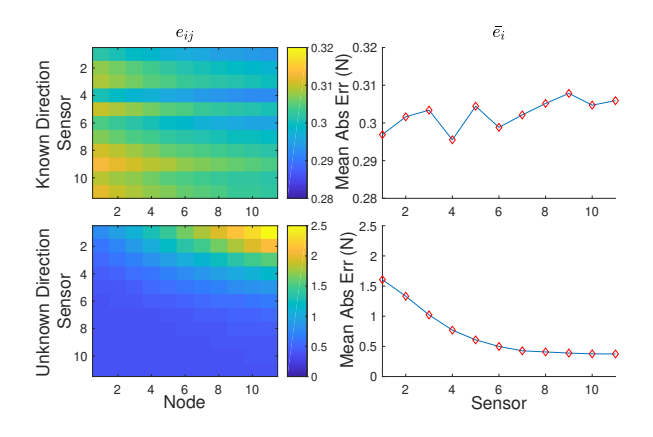


Fig. 8. Estimated vs. true tension using single-sensor estimation for two iterations (rows), when the direction of motion is known (top), or unknown (bottom). Lines indicate the mean of 2000 repetitions, shaded areas indicate the 95% confidence interval.

was at node i, which can be seen in Fig. 9, and the betweennode average, for each sensor,  $\bar{e}_i$ .

Results show that the estimation error is not sensitive to sensor location for the known direction case, as described in Sec. IICx, while estimation error decreases when sensors are distal along the cable in the unknown direction case, with mean sensor values of 0.37 N for sensor 11 compared to 1.6 N for sensor 1. The estimated functions  $\bar{e}_i$  were used for the weighted average procedure described in Sec IIC.

- 2) Sensor fusion: We tested separately the different sensor fusion methods based on whether the direction of motion is known, or unknown.
- a) Direction of motion known: For all sensing conditions, the logic used for estimating the tension and displacement profiles is a simple average of the estimates provided by each sensor, as described in Sec. IIC. Results from the three configuration options overlapped as a function of the number of sensors as reported in Fig. 10. In this case, the error is only determined by the number of sensors used, and it is independent of their location, with the difference between configurations less than 0.01 N, which has negligible on the overall estimation error.
- b) Direction of motion unknown: Because estimation accuracy are likely affected by the "true" motion condition, we considered separately two cases, one where the cable is in mass motion, and the other one, where the cable is in partial motion.

Mass Motion - We applied the sensor fusion methods discussed in Sec. IIC to the three configuration options, and repeated state estimation using 2000 simulated sensor measurements, in the same two iterations described above (Fig. 10), corresponding to a mass motion condition.

Results of the mass-motion analysis are displayed in Fig. 11, which reports the average estimation error across the 2000 repetitions. Results indicate that error decreases with the number of sensors for all configurations and sensing modes, as expected (average improvement between 1 and 11 sensors: 0.35 N). When comparing errors measured with different configurations but under the same number of

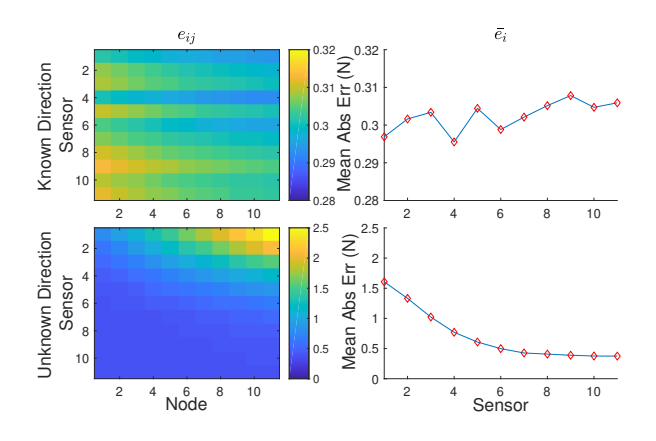


Fig. 9. (Left) Absolute error  $e_{ij}$  measured at node j using a a sensor located at node i for the known direction case (top), and the unknown direction case (bottom). (Right) Between-node mean of absolute error  $\bar{e}_i$ . Note the scales for both rows are different.

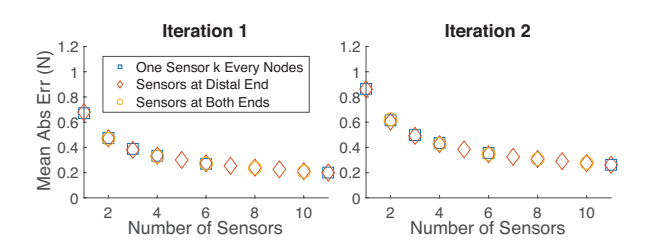


Fig. 10. Estimation error in the known direction of motion case for two iterations (columns), as a function of the number of sensors and their location. Iterations are the same as those considered in Fig. 8

sensors, errors in the Distal configuration are consistently smaller than the corresponding ones obtained with the other two options (average improvement of 0.2 N between Distal and Even and 0.07 N between Distal and Both). The decrease in error as a function of number of sensors is smaller when using the Distal configuration, compared to the other two (Distal: 0.02 N, Even: 0.67 N, Both: 0.37 N). As per Fusion method, the smallest error is afforded by the W Mean method (W Mean: 0.42 N, Mean-R: 0.47 N, Mean: 0.49 N, W Mean-R: 0.57 N).

For the optimal sensing condition (Distal), however, the best results are obtained using the Mean or W Mean fusion methods when using a low number of sensors (2-5) (mean error: 0.38 N for both), while the simple Mean fusion method affords the most accurate estimation when using a high number of sensors (6-11) (mean error: 0.33 for Mean, 0.35 for W mean).

Based on this analysis, there is little support for advanced fusion methods such as the weighted mean, or those based

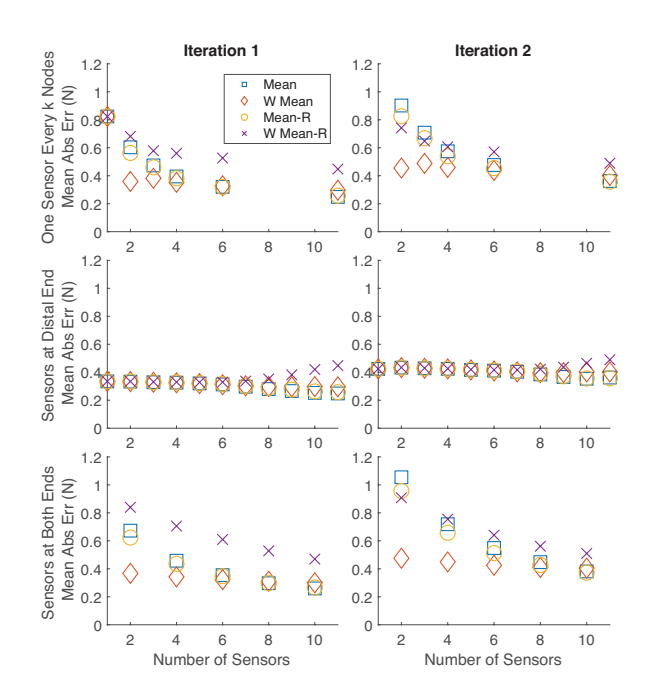


Fig. 11. Estimation error in the unknown direction case for two iterations (columns), as a function of the number of sensors (x axis), their location (rows), and estimation method (overlay). Iterations are the same as those considered in Fig. 8.

on removal of certain sensors, provided that sensors can be employed to measure tension in the distal nodes. Overall, it appears very important to be able to instrument the distal nodes: estimation error obtained in the Distal configuration using m sensors is similar (within 0.01 N) to the one obtained in the Both configuration with 2m sensors - suggesting that proximal tension measurements introduce negligible improvement in estimation capabilities.

Partial Motion - We then tested whether the presented estimation methods would provide accurate estimates of the system states also when the system was not in mass motion (partial motion). As such, we simulated 2000 repeated estimations of the system states at two iterations, where the last moving node was at node 8, and motion was only present in the proximal location of the cable (true value of tension profile shown in Fig. 12, top rows). We included all sensor configurations reported above, with the exception of the Distal configuration. This configuration was not implemented here due to the fact that the sole use of distal sensors would not help with state estimation, as sensors would fall in a stationary region of the cable and not be usable to estimate cable tension.

Results of the partial motion analysis are reported in Fig. 12, which reports the average estimation error across the 2000 repetitions. Results indicate that error decreases with the number of sensors for all unweighted sensing modes (average improvement between 1 and 11 sensors: 0.17 N Unweighted vs -5.6 N Weighted).

When comparing errors measured using different sensing

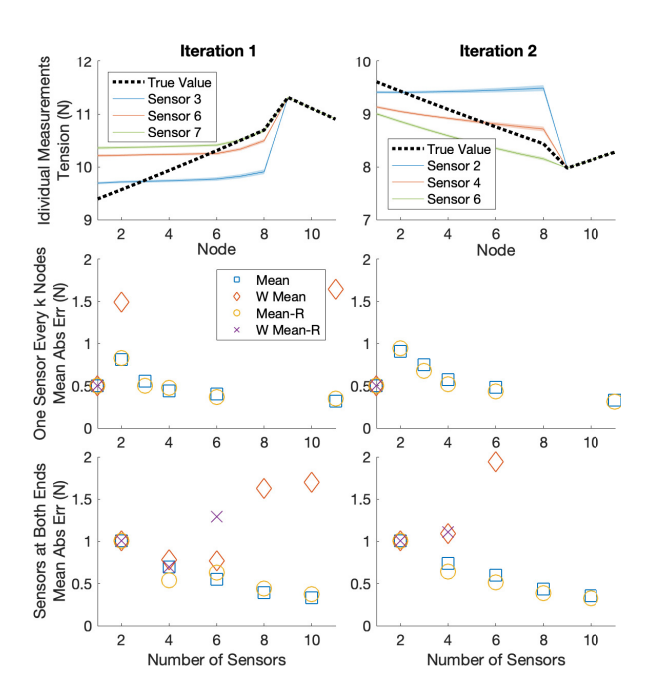


Fig. 12. State estimation during partial motion. (top) Estimated vs. true tension using single-sensor estimation for two iterations (rows). (center and bottom) Estimation error in the unknown direction as a function of the number of sensors (x axis), their location (rows), and estimation method (overlay). The Distal configuration is removed due to the potential for motion sections to have no distal nodes.

configurations under the same number of sensors, errors in the Even configuration are smaller than the corresponding ones obtained with the Both configuration in all UW conditions, while they are larger in the W conditions (average improvement of 0.15 N in Even compared to Both in UW conditions, average improvement of 6.4 N in Both compared to Even in W conditions).

As per fusion method, the smallest error is afforded by the Mean-R method (W Mean: 4.7 N, Mean-R: 0.52 N, Mean: 0.54 N, W Mean-R: 5.9 N) across sensing configurations.

Overall, optimal estimation conditions are obtained under the Even sensing condition and Mean-R processing method (estimation error: 0.53 N), but similar performance is obtained under the Mean method (estimation error: 0.55 N).

Findings obtained via the partial motion analysis are not fully in agreement with those obtained in the mass motion analysis. In both cases, the simple Mean sensor fusion method performs optimally or close-to-optimally. However, the sensing configuration Even, which is not efficient for mass motion, affords the best estimation performance in the partial motion analysis.

#### IV. DISCUSSION AND CONCLUSION

We have developed and validated a novel cable-conduit transmission model capable of describing interaction of robots with active environments. The simulated model was determined to be accurate, computationally faster than standard nonlinear models, and effective as a state estimator.

Regarding the model accuracy, the simulated results of our model qualitatively match effects observed in experiments conducted with a benchtop cable-conduit transmission prototype involving non-passive human interaction.

While the model was sufficiently accurate, its formulation based on a set of nonlinear differential equations made it difficult its integration in real-time simulators needed for model-based feedback control, or for real-time sensing of the cable configuration. To overcome this limitation, we developed a new form of an iterative linear solver, based on assumption of directions of motion for all cable segments, solution of the linear system of equations given the assumptions, and final evaluation of whether the obtained solution is compatible with the assumed directions of motion. The iterative linear solver showed to be accurate in solving the system equations, with the difference between the linear and nonlinear solver within machine precision ( $10^{-9}$  N). The main advantage of the developed iterative linear solver is that this formulation provided a considerable increase in computation speed (roughly two orders of magnitude) compared to nonlinear solvers, capable of running a 40segment cable in real-time at 1kHz.

Finally, regarding the possibility of using the model to perform sensor fusion and estimate in real time the states of the transmission, our analysis showed that under realistic sensor noise conditions (10% error), the model can be used to estimate the states with acceptable accuracy using simple algorithms that integrate measurements from multiple sensors distributed along the cable.

As per optimal sensing and estimation methods, it was observed that the best method for fusing individual sensor measurements was the sample mean. Based on our analysis, it is not obvious which is the optimal sensor configuration condition. Under mass motion, the optimal sensor configuration resulted to be the one with most sensors located in the distal end of the cable, while under partial motion (proximal side of the cable moving), the optimal sensor configuration turned to be the one with evenly distributed cable. This result is in part expected given the fact that when a section of the cable is stationary, the model can not make use of tension reading (expected to be constant) from those sensors to solve for the system states.

The model is not without limitations. Some of the observed inaccuracy can be attributed to the simplified friction model. We expect that including friction models specifically designed for cable-conduit transmissions [17] will allow for more accurate predictions of engagement behavior as well as capture trends resulting from other unmodeled frictional effects. While the inclusion of more advanced friction models, such as the inclusion of viscous friction, was shown in previous work to provide more accurate predictions of engagement behavior of a physical system, the estimator and model are robust enough to capture the desired behavior of the system while minimizing model complexity. Furthermore, allowing for variable-length segments as a function of their instantaneous radius of curvature will allow for optimization of the computational complexity of the model. This will be of benefit for wearable applications, where regions of large curvature are usually only near human joints.

Future work involves integrating this model and available sensor technologies into a state estimator to be used in real-time control applications, and developing new sensing techniques to further take advantage of the computational capabilities now available.

# V. ACKNOWLEDGMENT

We acknowledge the contribution of Andrew Borowski in developing the first version of the model and linear solver, and conducting exploratory analyses on state estimation.

# REFERENCES

- [1] R. C. Browning, J. R. Modica, R. Kram, and A. Goswami, "The effects of adding mass to the legs on the energetics and biomechanics of walking," *Medicine and Science in Sports and Exercise*, vol. 39, no. 3, pp. 515–525, 2007.
- [2] M. Kaneko, W. Paetsch, and H. Tolle, "Input-dependent stability of joint torque control of tendon-driven robot hands," *IEEE Transactions* on *Industrial Electronics*, vol. 39, no. 2, pp. 96–104, apr 1992.
- [3] A. T. Asbeck, R. J. Dyer, A. F. Larusson, and C. J. Walsh, "Biologically-inspired soft exosuit," in *IEEE International Conference on Rehabilitation Robotics*. IEEE, jun 2013, pp. 1–8.
- [4] J. Zhang, C. C. Cheah, and S. H. Collins, "Experimental comparison of torque control methods on an ankle exoskeleton during human walking," in 2015 IEEE International Conference on Robotics and Automation (ICRA). IEEE, may 2015, pp. 5584–5589.
- [5] K. Heer, J. Lee, N. Collins, M. Auger, and O. Celik, "Design and Control of a Modular Lower-Limb Exoskeleton Emulator for Accelerated Design and Evaluation of Assistive Gait Exoskeleton Parameters," in Proceedings of the 41st Annual Meeting of the American Society of Biomechanics, 2017, pp. 475–476.

- [6] L. Cappello, D. K. Binh, S. C. Yen, and L. Masia, "Design and preliminary characterization of a soft wearable exoskeleton for upper limb," Proceedings of the IEEE RAS and EMBS International Conference on Biomedical Robotics and Biomechatronics, vol. 2016-July, p. 8, 2016.
- [7] J. F. Veneman, R. Ekkelenkamp, R. Kruidhof, F. C. T. Van Der Helm, and H. Van Der Kooij, "Design of a series-elastic and bowdencable-based actuation system for use as torque-actuator in exoskeleton-type training," in *Proceedings of the 2005 IEEE 9th International Conference on Rehabilitation Robotics*, vol. 2005. IEEE, 2005, pp. 496–499.
- [8] F. Sergi, A. Erwin, B. Cera, and M. K. O'Malley, "Compliant force-feedback actuation for accurate robot-mediated sensorimotor interaction protocols during fMRI," 5th IEEE RAS/EMBS International Conference on Biomedical Robotics and Biomechatronics, pp. 1057–1062, aug 2014.
- [9] A. Schiele, P. Letier, R. Van Der Linde, and F. Van Der Helm, "Bowden cable actuator for force-feedback exoskeletons," *IEEE International Conference on Intelligent Robots and Systems*, pp. 3599–3604, 2006.
- [10] W. Townsend and J. Salisbury, J., "The Effect of coulomb friction and stiction on force control," *Proceedings. 1987 IEEE International Conference on Robotics and Automation*, vol. 4, pp. 883–889, 1987.
- [11] T. N. Do, T. Tjahjowidodo, M. W. S. Lau, and S. J. Phee, "Position control of asymmetric nonlinearities for a cable-conduit mechanism," *IEEE Transactions on Automation Science and Engineering*, vol. PP, no. 99, pp. 1515–1523, jul 2015.
- [12] Q. Wu, X. Wang, L. Chen, and F. Du, "Transmission Model and Compensation Control of Double-Tendon-Sheath Actuation System," *IEEE Transactions on Industrial Electronics*, vol. 62, no. 3, pp. 1599– 1609, mar 2015.
- [13] Y. Jung and J. Bae, "Torque control of a double tendon-sheath actuation mechanism in varying sheath configuration," in 2017 IEEE International Conference on Advanced Intelligent Mechatronics (AIM). IEEE, jul 2017, pp. 1352–1356.
- [14] M. Kaneko, M. Wada, H. Maekawa, and K. Tanie, "A new consideration on tendon-tension control system of robot hands," 1991 IEEE International Conference on Robotics and Automation (ICRA), no. April, pp. 1028–1033, 1991.
- [15] G. Palli and C. Melchiorri, "Model and control of tendon-sheath transmission systems," in *Proceedings IEEE International Conference on Robotics and Automation*, vol. 2006. IEEE, 2006, pp. 988–993.
- [16] T. N. Do, T. Tjahjowidodo, M. W. S. Lau, and S. J. Phee, "Dynamic Friction-Based Force Feedback for Tendon- Sheath Mechanism in NOTES System," *International Journal of Computer and Electrical Engineering*, vol. 6, no. 3, pp. 252–258, 2014.
- [17] T. N. Do, T. Tjahjowidodo, M. W. Lau, and S. J. Phee, "A new approach of friction model for tendon-sheath actuated surgical systems: Nonlinear modelling and parameter identification," *Mechanism and Machine Theory*, vol. 85, pp. 14–24, 2015.
- [18] V. Agrawal, W. J. Peine, and Bin Yao, "Modeling of a closed loop cable-conduit transmission system," in 2008 IEEE International Conference on Robotics and Automation. IEEE, may 2008, pp. 3407– 3412.
- [19] V. Agrawal, W. J. Peine, and B. Yao, "Modeling of Transmission Characteristics Across a Cable-Conduit System," *IEEE Transactions* on *Robotics*, vol. 26, no. 5, pp. 914–924, oct 2010.
- [20] A. Roberts, K. Thorn, M. L. Michna, N. Dragomir, P. Farrell, and G. Baxter, "Determination of bending-induced strain in optical fibers by use of quantitative phase imaging," *Opt. Lett.*, vol. 27, no. 2, pp. 86–88, Jan 2002.
- [21] U. Jeong and K.-J. Cho, "A Novel Low-Cost, Large Curvature Bend Sensor Based on a Bowden-Cable," *Sensors*, vol. 16, no. 7, p. 961, jun 2016.
- [22] E. T. Thostenson and T. W. Chou, "Carbon nanotube networks: Sensing of distributed strain and damage for life prediction and self healing," *Advanced Materials*, vol. 18, no. 21, pp. 2837–2841, 2006.
- [23] L. H. Blumenschein, C. G. McDonald, and M. K. O'Malley, "A cable-based series elastic actuator with conduit sensor for wearable exoskeletons," in 2017 IEEE International Conference on Robotics and Automation (ICRA). IEEE, may 2017, pp. 6687–6693.
- [24] A. Borowski, A. Metz, and F. Sergi, "Dynamic model of cable-conduit actuation for interaction with non-passive environments," in 2018 IEEE Haptics Symposium (HAPTICS). IEEE, mar 2018, pp. 40–45.

# APPENDIX I: DERIVATION OF THE NUMBER OF PERMUTATIONS FOR LINEAR ITERATIVE SOLVER

We here provide a derivation for the result described in Sec. IIB, where the total number of feasible permutations of velocity sign values within the cable  $n_p^*$ , was determined as,

$$n_p^* = 2N + 1 + \sum_{i=1}^{N-1} 4j \tag{8}$$

A cable can either be in mass motion or in partial motion. Partial motion can result from motion on only one side of the cable, or motion of both sides of the cable with a stationary section of the cable in the center. Given a number of segments N, there are 2N configurations for mass motion. In fact, the direction of motion may not change at all (1 condition), or it may change within the cable at either of the segments from 2 to N (N-1 conditions), and there are two directions of motion. Also, there is one configuration where the entire cable is stationary. The number of configurations associated with partial motion are instead given by the summation term included in (8), a described below.

In fact, there are 4(N-1) configurations where only one side of the cable is stationary. These configurations result from the fact that there exist N -1 choices for the last moving segment, with two choices for side of cable and direction of motion of the moving section. Using a similar argument, proceed to count recursively the number of configurations where the two extremal sections of the cable are in motion, and a central section is stationary. In fact, there are 4(N-2)configurations where one central segment is stationary (N-1)choices for the stationary segment in the center, 2 choices for direction of motion and side of cable with positive direction), 4(N-3) choices where two segments are stationary, giving the final summation term of 4\*1 (1 choice for the entire central section of the cable stationary -N-2 segments with the two extremal segments moving in any combination of direction). The combination of all the terms listed above is given in (8).

# APPENDIX II: CORRESPONDENCE BETWEEN SOLUTIONS OF LINEAR AND NON-LINEAR SOLVERS

To begin proving the solution method, we first recall the exact nature of the model equations. There are two types of equations, those solely in tension variables, and those both in tension and displacement variables.

We will start focusing on the n equations in n+1 unknowns, the  $T_i$  states, that only include tension variables. By our problem setup, we ensure we have at least one tension known<sup>2</sup>. The n equations take the general form

$$0 = T_i f(\operatorname{sign}(\operatorname{mean}(u_{i,t} - u_{i,t-1}, u_{i+1,t} - u_{i+1,t-1}))) - T_{i+1}$$
(9)

<sup>2</sup>We permit position-position to be an input as well. However, we can proceed assuming we know at least one variable without losing generality since we ensure our full system has enough constraints to fully define the unknowns. Specifically, Position-Position provides information about tensions through the position equation

where f is an arbitrary nonlinear function,  $T_i, u_{i,t}$  are tension and displacement state variables at the discrete time instant t. The important feature of this functional form is that all states appearing inside a nonlinear function are within a sign function as well.

Given our specific functional form, and the nature of the sign function, it's apparent that Eqn. 9 can only take the forms given by

$$0 = T_i f(k_{i,j}) - T_{i+1} \tag{10}$$

where  $k_{i,j}$  is the value resulting from the sign function having value j for segment i. Let us assume every possibility for the arguments of the nonlinearity. For a two-node system, the following options are admissible:

$$0 = f(1)T_i - T_{i+1}$$
  

$$0 = f(0)T_i - T_{i+1}$$
  

$$0 = f(-1)T_i - T_{i+1}$$
(11)

Choosing assumption  $j=[k_{1,j},k_{2,j},...,k_{N,j}]$  from the set of all possible assumptions spanning allowable permutations of the sign functions, we place the equation in matrix form then augment with the constraint from the known value,  $T_1=\tau$ , to give us the linear system

$$\begin{bmatrix} 0 \\ \tau \end{bmatrix} = \begin{bmatrix} f(k_{1,j}) & -1 \\ 1 & 0 \end{bmatrix} \cdot \begin{bmatrix} T_1 \\ T_2 \end{bmatrix} \tag{12}$$

which, for our system, has the straightforward solution for a given assumption j

$$T_{1,j} = \tau$$
  
 $T_{2,j} = f(k_{1,j})\tau$  (13)

We then refer this closed-form solution to our other set of equations dealing in node displacements (Given in the second half of Eqn. 11) to obtain node displacements corresponding to assumption j, and use these displacements to calculate values for the quantity we previously assumed the sign of, segment velocity.

Now, we can compare our assumed values under assumption j to the true value. We require only that for every segment i, the assumed signs,  $k_{i,j}$  equal their post calculated values,  $k_{i,j} = k_{i,j}^+$ . When this condition is true, we have equivalence, for each i, of the nonlinear system equations and our simplified system, since

$$f(\text{sign}(\text{mean}(u_{i,t} - u_{i,t-1}, u_{i+1,t} - u_{i+1,t-1}))) = f(k_{i,j})$$
(14)

This is a consequence of what the assumption means: when we assume motion is toward the proximal end, friction must act toward the distal end, and in the absence of other forces, this means that tension increases over the segment. Mathematically, this manifests itself by the exponential quantity being greater than 1. When we assume motion toward the distal end, the inverse is true and the argument to the exponential being negative makes it output a quantity less than one.

If our assumption was incorrect, the solution obtained for the position equation would contradict with the information about tensions gained via assumption, and the model will produce node velocities that imply segment velocities whose signs do not match those previously assumed.

To prove the uniqueness of our solution, assume a single segment, bounded by two nodes, of some cable moving in the positive direction at the current time instant (i.e.  $S_1=1$ ). We measure a tension  $\tau$  at the input, and a displacement from 0 to x between the previous and current timestep at the output. Let us incorrectly choose to assume the cable moved in the negative direction (i.e  $S_1=-1$ ). Then 1>f(-1). From our position equations, we have

$$0 = u_1 - x + \tau \frac{R}{k_c \mu} (S_1)(f(-1) - 1)$$

$$\to u_1 = x - \tau D_{1,-1}$$
(15)

where D is a positive constant combining all terms in the tension coefficient,  $\frac{RS_i}{k_c\mu}(f(-1)-1)$ . We calculate the sign of the velocity's segment as

$$\begin{aligned} & \operatorname{sign}(v_1) = \operatorname{sign}(\frac{1}{2}(u_{1,t} - u_{1,t-1}) + (u_{2,t} - u_{2,t-1})) \\ & \operatorname{sign}(v_1) = \operatorname{sign}(((x - \tau D_{1,-1}) - u_{1,t-1}) + (x - 0)) \end{aligned} \tag{16} \\ & \operatorname{sign}(v_1) = \operatorname{sign}(2x - \tau D_{1,-1} - u_{1,t-1}) \end{aligned}$$

However, we can place a conservative upper bound on both quantities on the right. Since the term  $\tau D_{1,-1}$  represents the change in length due to the frictional losses in a segment, if  $\tau D_{1,-1} \geq x$  then that cable segment would be slack at the current time, since the displacement of both nodes relative to the segment is toward the middle. This is a contradiction if  $\tau \neq 0$ , the presence of that measurement means the cable is not slack; and if  $\tau = 0$ , this term still obeys our desired bound (since it is identically zero). Fig. S1 visualizes this relationship. Since Node 2's position is known, when we visualize this relationship, it becomes clear that violation of the stated bound results in a segment length less than the slack length. Therefore, it is true that  $\tau D_{1,-1} < x$ .

We could present a similar appeal to bound  $u_{1,t-1}$ , but there is a stronger argument available. Consider the state of

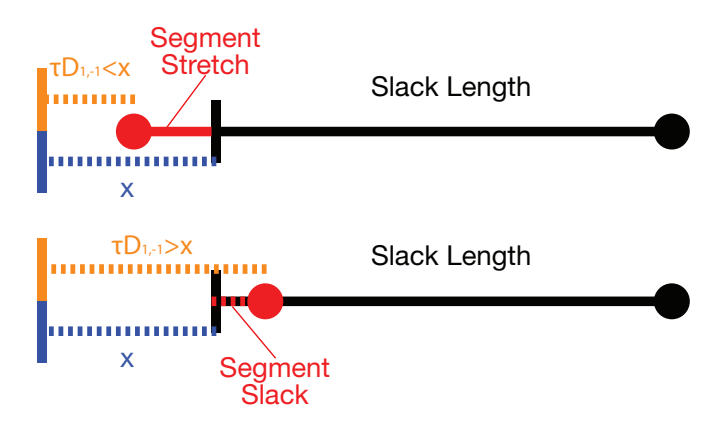


Fig. S1. Visualization of the bounding of the quantity  $\tau D_{1,-1}$ . When the quantity exceeds the bound, the final length of the cable segment is less than its rest length and is therefore slack. This contradicts the fact that  $\tau$  used to calculate this quantity is nonzero, and thus claims that the cable is not slack.

the cable at the previous time: we have defined our coordinate system such that  $u_{2,t-1} = 0$ . Let's align this to a coordinate system  $\bar{x}$  of the true position of a node with respect to the conduit, rather than relative displacements, such that  $\bar{x}_{2,t-1} = 0$  as well. In this coordinate system,  $\bar{x}_{1,t-1} =$  $u_{1,t-1} - L_{segment}$ , where  $L_{segment}$  is the cable segment's slack length. The current length of the segment is expressed as  $\bar{x}_{2,t-1} - \bar{x}_{1,t-1} = (0) - (u_{1,t-1} - L_{segment})$ . For the cable to be non-slack, we require that  $\bar{x}_{2,t-1} - \bar{x}_{1,t-1} \ge L_{segment}$ . Clearly this is only the case when  $u_{1,t-1} \leq 0$ . Therefore, with frames defined as we have here, the previous position of Node 1,  $u_{1,t-1}$  is strictly nonpositive since the model cannot produce slack segments. Fig. S2 visualizes this relationship. Since choosing a different reference frame in this 1-D system results only in offsetting all quantities by a constant, we can extend this result to any frame without loss of generality.

Therefore, if we define  $\gamma \equiv \tau D_{1,-1} + u_{1,t-1}$  we can state the inequality  $\gamma < x$  and simplify the equation above into

$$sign(v_1) = sign(2x - \gamma) 
sign(v_1) = 1$$
(17)

This is a contradiction on the incorrectly made assumption that  $sign(v_1) = -1$ .

We can trivially reject the second possible incorrect assumption of  $\operatorname{sign}(v_1)=0$ , by appealing to the changes in measured tensions and positions. Recall that when a segment is not in motion, its state variables are retained from the previous time step. However, our closed-form solution here indicates that  $u_1=u_2$  if  $k_{1,j}=0$ . This is in general a contradiction of its own, unless x=0 and  $u_{1,t-1}=0$ , which alternatively contradicts our construction that the true motion was in the positive direction.

Since the proof has symmetry with the opposite motion case, we can be assured that this mathematical formulation rejects incorrect assumptions made in either direction.

Additionally, since there can only be one true solution of the non linear system, and we have equivalence of any valid assumption scheme and the original non linear system, we know that once we find a single valid solution, all other solutions will be invalid and we can stop without considering unchecked solutions.

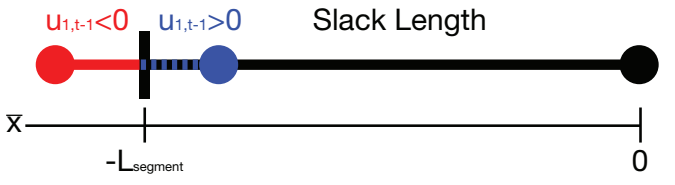


Fig. S2. Visualization of the bounding of the quantity  $u_{1,t-1}$ . If this quantity were to take on any positive value, the length of the segment would be less than its rest length at the previous time, and therefore slack.